Aqueous Ferrofluid of Magnetite Nanoparticles: Fluorescence Labeling and Magnetophoretic Control

Yudhisthira Sahoo,[†] Alireza Goodarzi,[‡] Mark T. Swihart,[‡] Tymish Y. Ohulchanskyy,[†] Navjot Kaur,[†] Edward P. Furlani, and Paras N. Prasad*,[†]

Department of Chemistry, Department of Chemical and Biological Engineering, Institute for Lasers, Photonics and Biophotonics, University at Buffalo (SUNY), Buffalo, New York 14260

Received: October 8, 2004

A method is presented for the preparation of a biocompatible ferrofluid containing dye-functionalized magnetite nanoparticles that can serve as fluorescent markers. This method entails the surface functionalization of magnetite nanoparticles using citric acid to produce a stable aqueous dispersion and the subsequent binding of fluorescent dyes to the surface of the particles. Several ferrofluid samples were prepared and characterized using Fourier transform infrared spectroscopy (FTIR), X-ray photoelectron spectroscopy (XPS), thermogravimetric analysis (TGA), BET surface area analysis, transmission electron microscopy (TEM), and SQUID magnetometry. In addition, confocal fluorescence microscopy was used to study the response of the fluorescent nanoparticles to an applied magnetic field and their uptake by cells in vitro. Results are presented on the distribution of particle sizes, the fluorescent and magnetic properties of the nanoparticles, and the nature of their surface bonds. Biocompatible ferrofluids with fluorescent nanoparticles enable optical tracking of basic processes at the cellular level combined with magnetophoretic manipulation and should be of substantial value to researchers engaged in both fundamental and applied biomedical research.

Introduction

There is substantial and growing interest in the development of magnetic nanoparticles for use in a broad range of applications that span both fundamental and applied research. The fundamental research involves the study of important physical phenomena such as superparamagnetism,[1] magnetic dipolar interactions,[2] single electron transfer,[3] and magnetoresistance.[4] The applied research has led to the integration of magnetic nanoparticles in a myriad of commercial applications including ferrofluids[5] and data storage devices.[6] Magnetic nanoparticles are also used in important biomedical applications. These include magnetic bioseparation of labeled cells and biological entities,[7] therapeutic drugs,[8] gene and radionuclide delivery,[9] radio frequency induced destruction of cells and tumors via hyperthermia,[10] and contrast enhancement agents for MRI.[11] Magnetic nanoparticles are well suited for these applications for several reasons. First, they can be selectively fabricated in sizes that range from several to hundreds of nanometers making them smaller than or comparable in size to important biological entities such as cells (10−100 μm), viruses (20−450 nm), proteins (3−50 nm), and genes (10-nm wide and 10−100-nm long).[12] Second, they can be surface-functionalized with biological molecules that enable selective interaction with various target bioentities.[13] Third, their motion can be manipulated and controlled by an external magnetic field.[14] Fourth, they can absorb energy from a time-varying magnetic field and dissipate it at the cellular level in the form of heat.[10]

A relatively recent enhancement of magnetic nanoparticle systems is the introduction of surface-bound fluorescent dyes. These dyes can be optically activated with the particles in situ. Upon activation, the dyes emit light that enables optical tracking of the particles using ordinary or two-photon confocal microscopy.[15] This, in combination with target-specific surface functionalization, provides a powerful tool for studying a variety of biological interactions at the cellular level.

It is a technological challenge to control the size, shape, and dispersibility of nanoparticles in desired solvents. Such particles have large surface-to-volume ratio and therefore high surface energies. Consequently, they tend to aggregate so as to minimize the surface energy. In addition to a high surface energy, magnetic nanoparticles experience interparticle dipolar attractions that tend to further destabilize a colloidal dispersion of them.[16] A suitable surface functionalization and choice of solvent are crucial to achieving sufficient repulsive interactions to prevent aggregation so as to obtain a stable colloidal solution of magnetic nanoparticles, a ferrofluid.

Among the various methods for producing nanoparticles, wet chemical routes have the advantages of being relatively simple and providing good control over particle properties. Introducing a suitable surfactant during or after the synthesis prevents aggregation of the nanoparticles and makes a stable colloidal dispersion possible. Most surfactants adhere to surfaces in a substrate-specific manner. For example, thiols bind to gold and silver surfaces, carboxylic acids bind to oxide surfaces, and nitriles and amines bind to platinum.[17] However, the mere presence of a functional group does not guarantee that a ligand will bind to the surface of a nanoparticle or that a stable dispersion will form. Often, the chain length and solvent system have significant influence on the formation of a truly stable dispersion. In the magnetic ferrite particles, the carboxylate ends of long-chain carboxylic acids such as oleic acid and stearic acid bind well to the particles so that the aliphatic chains extending out from their surface of the particle make them

* Corresponding author. Tel: (716)645-6800 x2098; e-mail: pnprasad@buffalo.edu.
[†] Department of Chemistry.
[‡] Department of Chemical and Biological Engineering.

10.1021/jp045402y CCC: $30.25
Published on Web 02/11/2005

effectively hydrophobic and dispersible in nonpolar solvents.[18] Sahoo et al.[19] have shown that alkyl phosphonates and phosphates also bind to magnetite particles well and render their surfaces hydrophobic. Shen et al.[20] have shown that intermediate length carboxylic acids from C_9-C_{12} can form a bilayer structure and make the surface hydrophilic, enabling formation of a stable aqueous dispersion.

Aqueous colloidal dispersions of magnetic nanoparticles hold great potential for use in a variety of new and existing bioprocesses because of the compatibility of the aqueous medium with biosystems. Specific applications include magnetic bioimaging and magnetocytolysis. The results presented below demonstrate that surface modification of magnetite particles by citric acid (CA) allows the formation of a stable aqueous dispersion. Moreover, the active carboxylate group on the surface of the particles makes them amenable to binding with fluorescent dyes. The resulting combination of magnetic and fluorescent properties opens a new gateway for a host of magnetophoretically controlled bioapplications.

Experimental Section

Materials. $FeCl_2 \cdot 4H_2O$ and $FeCl_3 \cdot 6H_2O$ were purchased from J. T. Baker; citric acid monohydrate (CA) from Fisher Chemicals; 1-[3-(dimethylaminopropyl)-3-ethylcarbodiimidehydrochloride (EDC) and (2-*N*-morpholinoethanesulfonic acid) (MES) from Sigma-Aldrich; and Rhodamine 110 from Molecular Probes.

Nanoparticle Synthesis. Magnetite particles were prepared by coprecipitation of Fe_3O_4 from a mixture of $FeCl_2$ and $FeCl_3$ (1:2 molar ratio) upon addition of NH_4OH. In a typical reaction, 0.86 g $FeCl_2$ and 2.35 g $FeCl_3$ were mixed in 40 mL water and heated to 80 °C under argon in a three-necked flask. While vigorously stirring the reaction mixture, 5 mL of NH_4OH was introduced by syringe, and the heating continued for 30 min. After that, 1 g of CA in 2 mL water was introduced, the temperature was increased to 95 °C, and stirring continued for an additional 90 min. A small aliquot of the reaction mixture was withdrawn, diluted to twice its initial volume, placed in a vial, and then subjected to a static magnetic field of several hundred Gauss. The particles remained dispersed in the fluid even in the presence of the external field indicating that a stable colloidal solution had formed.

Dialysis. The as-formed reaction product contains an excess of citric acid. Therefore, the nanoparticle dispersion was subjected to dialysis against water using a 12−14 kD cutoff cellulose membrane (Spectrum Laboratories, Inc., USA) for 72 h to remove the excess unbound CA.

Fourier Transform Infrared (FTIR) Spectroscopy. FTIR spectra were taken of neat citric acid, coated magnetite particles, and rhodamine dye-bound magnetite particles in KBr pellets. These measurements were made using a Perkin-Elmer FTIR spectrometer model 1760X operating in transmission mode.

X-ray Photoelectron Spectroscopy (XPS). XPS studies were performed on a Physical Electronics/PHI 5300 X-ray photoelectron spectrometer with a hemispherical analyzer and a single-channel detector that was operated at 300W (15 kV and 20 mA). Mg Kα radiation (1253.6 eV) and pass energies of 89.45 eV for survey scans and 17.9 eV for high-resolution scans were used.

Thermogravimetric Analysis (TGA). The TGA spectrograms were taken on a Perkin-Elmer instrument model TGA7. Typically, 5 mg of the sample was weighed into a sample compartment that was dried and flushed with ultrapure Argon. The spectrograms were collected at a heating rate of 5 °C/min up to 800 °C.

BET Surface Area Analysis. Nitrogen physisorption (the BET method) was performed to determine the specific surface area of the particles using a Micromeretics Model 2010 ASAP physiosorption apparatus.

Transmission Electron Micrographs (TEM). TEM were obtained using a model JEOL 100 CX II microscope at an acceleration voltage of 80 kV in the bright field image mode. Samples were prepared for TEM imaging by evaporating multiple drops of the clear dispersion onto a carbon-coated copper grid (300 mesh, Electron Microscopy Sciences).

Magnetization. DC magnetization measurements were made using a superconducting quantum interference device (SQUID) MPMS C-151 magnetometer from Quantum Design. The aqueous sample was placed in a nonmagnetic capsule that was then wrapped with layers of Teflon tape to prevent breakage under vacuum. The magnetic field was ramped from 0 to 10 000 G at both 300 and 5 K. At 5 K, the sample medium was frozen, but there was enough room left in the capsule to accommodate the expansion of water upon freezing.

Electrophoresis. A horizontal gel system with 2.5% agarose gel was used in the electrophoresis experiments. MP−CA and MP−CA−dye particles of equal concentration were run in parallel channels while applying a dc voltage of 80 V for 1 h.

Fluorescent Dye Binding and Fluorescence Spectroscopy. The fluorescent dye Rhodamine 110 was bound to the surface of the MP−CA particles following standard procedures for linking this dye to a carboxyl group.[21] Briefly, a concentrated dispersion of magnetic particles with practically no free citric acid was prepared in a 25 mM aqueous (2-*N*-morpholinoethanesulfonic acid) (MES) buffer. The amount of citric acid in 2 mL of the dispersion was estimated to be 0.2 mmol. To it was added 0.076 g (∼4 mmol) of (1-[3-(dimethylaminopropyl)-3-ethylcarbodiimidehydrochloride (EDC) followed by 0.009 g (0.25 mmol) of rhodamine 110 dye and the reaction vial was vortexed for 4 h. The resulting dye-linked particles were washed several times through alternate cycles of sonication and centrifugation to remove any unbound rhodamine dye. The steady-state fluorescence, as well as fluorescence anisotropy spectra, were acquired using a Fluorolog-3 spectrofluorometer (Jobin Yvon).

In Vitro Studies of Nanoparticle Uptake and Imaging. KB cells (ATCC, Manassas, VA) were maintained in a DMEM medium with 10% fetal bovine serum (FBS) according to ATCC instructions. For the nanoparticle uptake and imaging studies, the cells were trypsinized, resuspended in medium at a concentration of 7.5×10^3 cells/mL, and replated into 60-mm culture plates (5.0 mL in each). Cells were then placed in an incubator overnight at 37 °C with 5% CO_2 (VWR Scientific model 2400, Bridgeport, NJ). The following day, the cells (∼50% confluency) were rinsed with phosphate-buffered saline (PBS), and 5 mL of fresh medium was replaced on the plates. Then, 50 μL of an aqueous dispersion of nanoparticles was added to appropriate plates and mixed gently. The treated cells were returned to the incubator (37 °C, 5% CO_2) for 1 h. After incubation, the plates were rinsed with sterile PBS, and 5.0 mL of fresh medium was added to each. The cells were incubated (37 °C, 5% CO_2) for 2 h. They were then directly imaged using a confocal laser scanning system (MRC-1024, Bio-Rad, Richmond, CA), which was attached to an upright microscope (Nikon model Eclipse E800). A water immersion objective lens (Nikon, Fluor-60X, NA = 1.0) was used for cell imaging. An argon ion laser (Spectra-Physics) was used as a source of

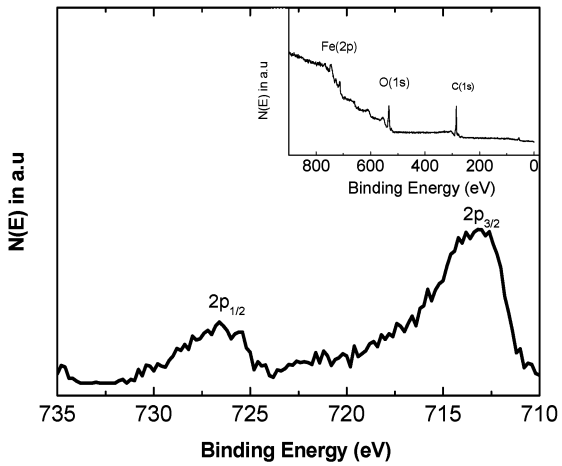

Figure 1. XPS spectrum of Fe in MP−CA showing the Fe 2p peaks. The inset is a survey spectrum representing the constituent elements in the sample.

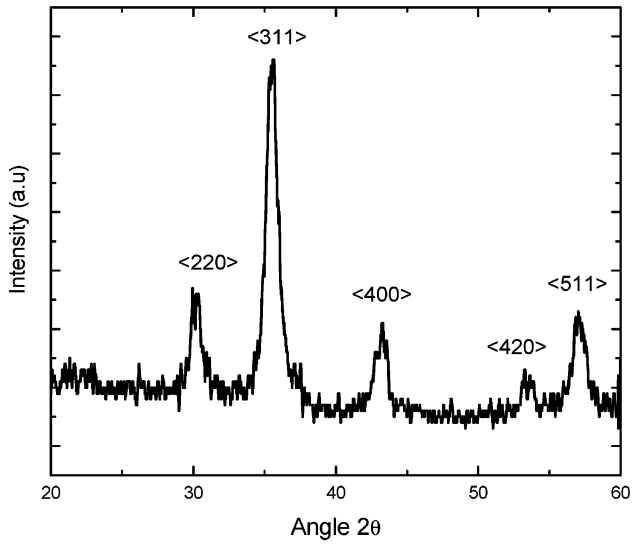

Figure 2. XRD spectrum of MP−CA powder. The fwhm of the 311 peak gives a particles size of ~10 nm.

excitation (488 nm), and a long-pass (585 LP) filter was applied as an emission filter for imaging.

Results and Discussion

The formation of Fe_3O_4 particles by coprecipitation of Fe^{2+} and Fe^{3+} by an alkali is well known and widely practiced.[18,19] There are many reports of long-chain carboxylic acid coated particles dispersible in organic nonpolar solvents.

X-ray photoelectron spectroscopy (XPS) (Figure 1) and X-ray diffraction (XRD) (Figure 2) results are consistent with the expected composition of Fe_3O_4 particles. The XPS shows that the binding energy of the Fe $2p_{3/2}$ shell electron is slightly above 710 eV, which is consistent with the oxidation state of Fe in Fe_3O_4.[23] The XRD peaks can be indexed into the spinel cubic lattice type with a lattice parameter of 8.34 Å. However, it cannot be determined from the XRD whether the further oxidized Fe_2O_3 phase exists in the sample because of the broad peaks, as are usually seen in nanoparticles. The expected intense peaks ⟨104⟩ at 33.220° of rhombohedral Fe_2O_3 and ⟨311⟩ at 30.108° of cubic Fe_3O_4 cannot be differentiated from one another in the XRD spectrum presented here.[24]

A TEM image of the as-prepared citric acid coated magnetite particles, without any size selection, is shown in Figure 3a. The

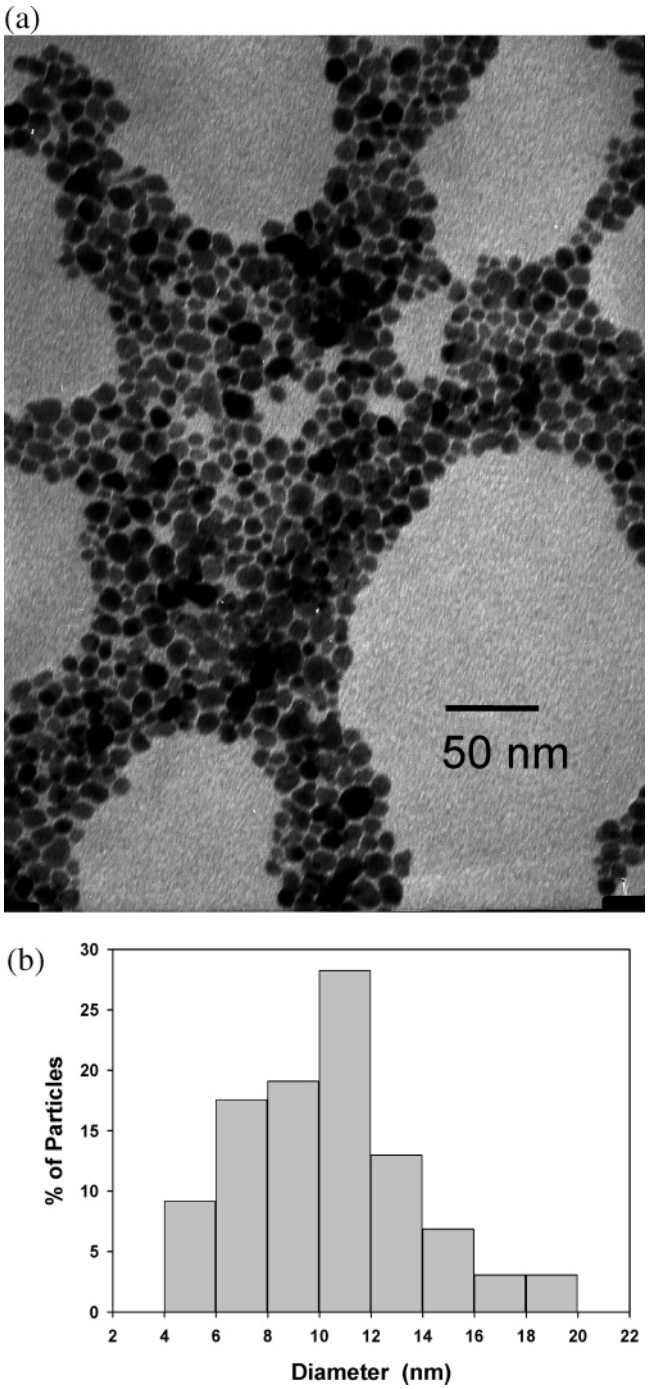

Figure 3. (a): TEM of magnetite nanoparticles MP−CA without size selection. The sizes range from 5 to 20 nm. (b): Size statistics of a polydisperse MP−CA sample.

sizes range from 4 to 20 nm with a dominant population at 10−12 nm (28%) (Figure 3b). By incrementally adding a relatively less polar solvent such as acetone or acetonitrile to the aqueous dispersion followed by centrifugation, size selective precipitation can be carried out. However, this size selection method is less effective in this case than for oleic acid coated magnetite particles or semiconductor nanoparticles dispersed in nonpolar solvents, as widely reported in the literature.

The XRD shows a finite broadening of the diffraction lines that provides an estimate of particle sizes from the Scherrer formula: $d_{\text{domain}} = 0.9\lambda/\beta \cos \theta$. For example, from the full width at half-maximum (fwhm) of the ⟨311⟩ peak of 0.017 rad for $\lambda = 0.154178$ nm and $\theta = 35.5°$, the particle size calculated

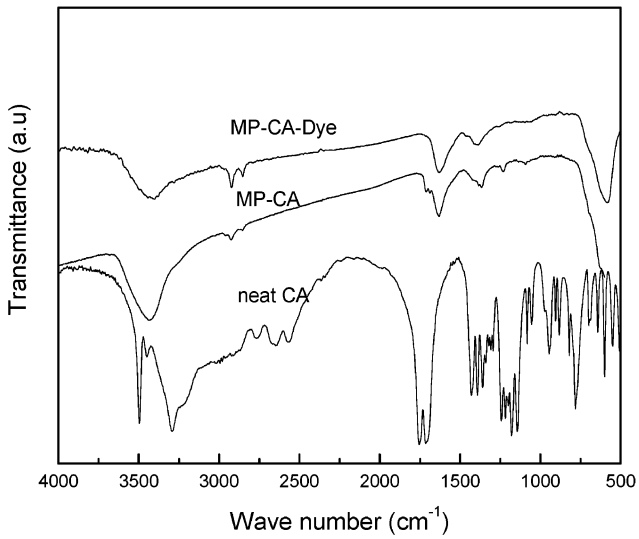

Figure 4. FTIR spectra of neat CA and MP−CA. The spectrum in MP−CA is mostly featureless, but the C═O and CH_2 stretching frequencies are recognizable.

from the formula is 10 nm, which is consistent with the average diameter observed in the TEM.

FTIR spectroscopy shows that the surface passivation of the particles occurs via the −COOH group. Figure 4 shows the FTIR spectra of the neat citric acid (CA), magnetite particles coated with citric acid (MP−CA), and the ones further bonded with dye (MP−CA−dye). The absorption bands for the neat CA are well resolved, but those of the MP−CA and MP−CA−dye are rather broad and few. The 1715 cm^{-1} peak assignable to the C═O vibration in neat CA is present as a broad band. Upon binding of CA to the magnetite surface, this band shifts to 1690 cm^{-1} in MP−CA. Carboxylate groups of CA should complex with the Fe atoms on the magnetite surface and render a partial single bond character to the C═O bond, weakening it, and shifting the stretching frequency to a lower value. This observation is similar to the citrate complex in $YFeO_3$ studied by Todorovsky et al.[25] It is proposed that CA binds to the magnetite surface by chemisorption of the carboxylate, that is, citrate ions. Earlier studies by Matijevic's group[26] have shown that oxalic acid and citric acid bind to the hematite surface through chemisorption that is highly pH dependent.[12] In their studies, zeta potential measurements indicated that citric acid is bound either as a bidentate or a tridentate ligand. From the FTIR features, it is undeterminable whether a covalent bonding of the −COOH group with rhodamine-110 dye has been accomplished. Hence, we must resort to other means of confirming that the dye has been intimately bound to the nanoparticles.

TGA results show a single-step weight loss for both neat CA and MP−CA (Figure 5). The weight loss in the latter case starts at a higher temperature and occurs more gradually than the weight loss for neat CA, which is quite sharp. CA does not have a normal boiling point because it decomposes before boiling at atmospheric pressure. There is approximately a 30 °C difference in the weight loss onset temperature (195° and 225 °C for the neat and MP−CA, respectively), which is an indicator of the enthalpy of adsorption of the CA molecules on the magnetite surface. Also, while the net weight loss for the neat CA is 100% as expected, the weight loss for MP−CA is 6%. We can attribute this to desorption of citric acid molecules from the surface of the magnetite particles. The mass of surfactant bound to the surface of the particles can be calculated as follows. If we assume a close-packed monolayer of the

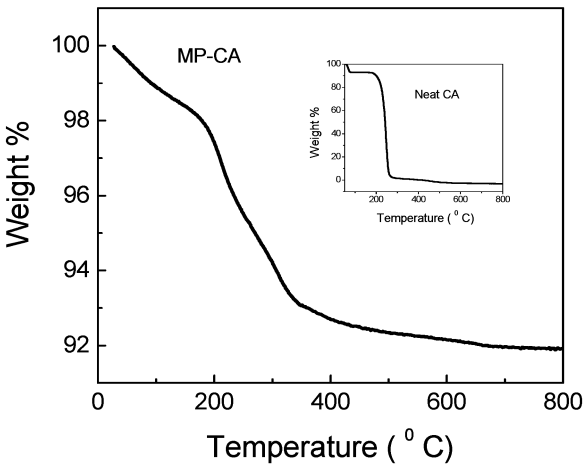

Figure 5. TGA curves of neat CA and MP−CA. The weight loss of the former is obviously 100% whereas that of the latter is ∼6%.

surfactant on the surface of a nanoparticle of diameter d_p, then the total weight of the nanoparticle plus the monolayer is $(1/6)\pi d_p^3\rho + (\pi d_p^2/a)(M/N_0)$, where ρ = the density of the particle, a = the head area per molecule of the surfactant, M = the molecular weight of the surfactant, and N_0 = Avogadro's number. Assuming that the TGA heating causes weight loss of only the surface-bound surfactant, the percentage weight loss from a particle of diameter d_p is $100 \times (4\pi d_p^2/a)(M/N_0)/((1/6)\pi d_p^3\rho + (\pi d_p^2/a)(M/N_0))$. For a polydisperse sample with a discrete size distribution $f(d_p)$, the fractional weight loss is obtained by summing over the size distribution as shown in eq 1

$$\text{weight loss fraction} = \frac{\sum_i (\pi d_{p,i}^2/a)(M/N_0) f(d_{p,i})}{\sum_i (1/6\pi d_{p,i}^3\rho + (\pi d_{p,i}^2/a)(M/N_0)) f(d_{p,i})} \quad (1)$$

Summing over the discrete nanoparticle size distribution fractions given in Figure 3b, with $\rho = 5.18$ g/cm^3, $a = 21$ Å^2, and $M = 192.12$ amu, gives the percentage weight loss for this particle size distribution as 4.7%. The experimentally observed ∼6% weight loss from the TGA curves is higher by only ∼28% (Figure 5). In the calculation, the assumed head area of 21 Å^2 is appropriate for a close-packed configuration of monodentate ligands.[18,27] In the case of citric acid as a ligand, there is a possibility of bidentate or tridentate binding depending on the affinity of the ligand to the surface of the nanoparticle and on steric effects. This would proportionately decrease the calculated weight loss and enhance the discrepancy. Therefore, the present result suggests that, despite repeated washing, more than a monolayer of surfactant is present, possibly because of hydrogen bonding among the citric acid molecules. Surfactant not bound to the particle surface, but held by interdigitation with the first monolayer, should in principle show an extra step in the TGA curve.[20] However, because of the strong hydrogen bonding in CA, the molecules might still remain bound and leave en masse on desorption giving rise to a single-step weight loss feature, as seen in the TGA curve.

The surface area measured by nitrogen physisorption (the BET method) was 75 m^2/g, which is somewhat smaller than the estimate of 93 m^2/g that one obtains from the size distribution shown in Figure 3b and a density of $\rho = 5.18$ g/cm^3. This discrepancy can possibly be explained by agglomeration

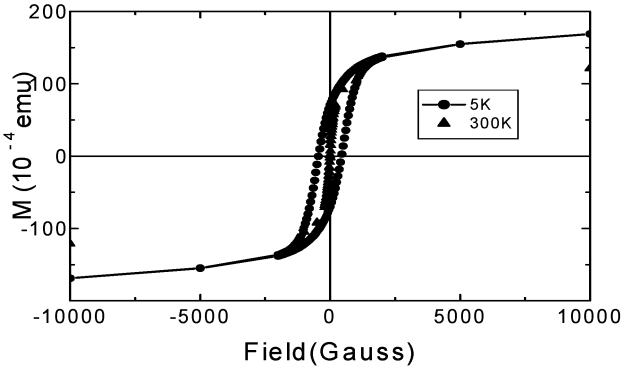

Figure 6. Magnetization of magnetite ferrofluid showing superparamagnetic behavior of the particles because of their small size.

of smaller particles to form larger ones, thereby effectively reducing the collective surface area. The problem of agglomeration in dried samples of the nanoparticles is particularly aggravated by the possibility of strong hydrogen bonding among the particle surfaces.

The CA coated particles forming the ferrofluid in this study are in their superparamagnetic regime. At 300 K, the magnetization of the sample, which was measured with an applied dc magnetic field of up to 10 000 G, shows saturation, but no hysteresis (Figure 6). However, when the same measurement is repeated at a temperature of 5 K, hysteresis appears with a coercive field of ~430 G, which suggests that the blocking temperature of the particles is above 5 K. For the current work, determination of the exact blocking temperature is not necessary. The superparamagnetic character of the particles is important for biomedical applications where a remanent magnetization is undesirable. For such applications, the particles must rapidly relax their magnetic moment vectors to random directions when the applied magnetic field is removed.

The fluorescence spectra from the dye-bound particles are shown in Figure 7a. With 490-nm excitation, a clear peak is observed at 520 nm. In one case, the dye was bound to the surface of the particles by the chemical reactions described above. These fluorescently tagged particles retain their fluorescence after multiple washings (by adding a less polar solvent such as acetonitrile or acetone followed by centrifugation) and redispersions of the precipitate (through sonication) (Figure 7a, curve 1). In this way, all the free dye has been removed. For the purpose of control, of course, when the rhodamine 110 was simply mixed with an aliquot of the MP−CA sample, it also exhibited fluorescence because of the free dye in the environment of the MP−CA dispersion (Figure 7a, curve 2). However, by imposing similar cycles of precipitation and redispersion on the latter mixture sample, the free dye is washed away, and the washed sample does not show any fluorescence (Figure 7a, curve 3). This test negates the possibility of the dye being strongly tagged to the negatively charged MP−CA surface by electrostatic forces and demonstrates the necessity of a chemical binding procedure. In Figure 7a, the binding of the dye to the nanoparticles surface causes a minor blue shift (~5 nm) of the maximum of the fluorescence band.

Another demonstration that the dye is indeed bound to the surface of a particle is presented in Figure 7b. The anisotropy of the fluorescence from a free rhodamine 110 solution and from a suspension of fluorescently labeled MP−CA particles was measured. Anisotropy in a spectrofluorometer is defined as $r = (I_{VV} - GI_{VH})/(I_{VV} + 2GI_{VH})$, where I_{VV}, I_{VH}, I_{HV}, and I_{HH} are emission intensities for different positions of excitation and emission polarizers; the first subscript indicates the position of the excitation polarizer, the second that of the emission polarizer. $G = I_{HV}/I_{HH}$ is a grating factor that must be included for correction in a monochromator.[28,29]

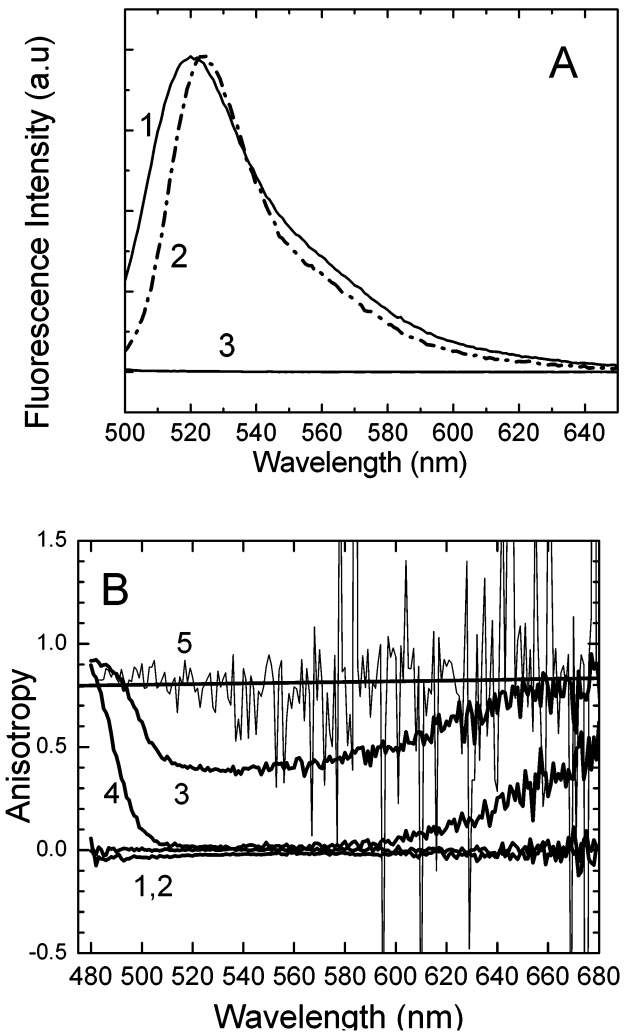

Figure 7. (a) Fluorescence spectra: (1) MP−CA tagged to rhodamine 110 dye and washed five times; (2) MP−CA mixed with rhodamine-110 dye; (3) sample 2 after washing twice. Chemically tagged MP−CA−dye conjugate retains its fluorescence even after multiple washings. (b) Fluorescence anisotropy: (1, 2) Rhodamine 110 water solution in a magnetic field (0.4 T) and without it; (3) MP−CA particles labeled with rhodamine 110; (4) MP−CA particles labeled with rhodamine 110 in magnetic field (0.4 T); 5 MP−CA particles without fluorescence labeling, linear fitting is applied.

The relative change in $r(\lambda)$ shown in Figure 7b clearly points to the binding of dye molecules and particles (curves 3, 4). As shown in Figure 7b, the free rhodamine 110 solution exhibits almost no fluorescence anisotropy, with or without the magnetic field applied (curves 1, 2). However, the fluorescence of the dye bound to the MP−CA particles manifests strong anisotropy that further increases in the presence of an applied magnetic field (curves 3, 4). This is understandable because of the limitation of the rotational mobility of rhodamine molecules bound to the particles.[30] Moreover, the applied magnetic field imposes an additional restriction on the movement of the particles and, correspondingly, on the movement of the dye molecules. The absolute value of anisotropy, which is experimentally measured in the spectrofluorometer, is sensitive to the excitation light that scatters off the sample. The anisotropy $r(\lambda)$ for the unlabeled MP−CA particles is shown in curve 5 of

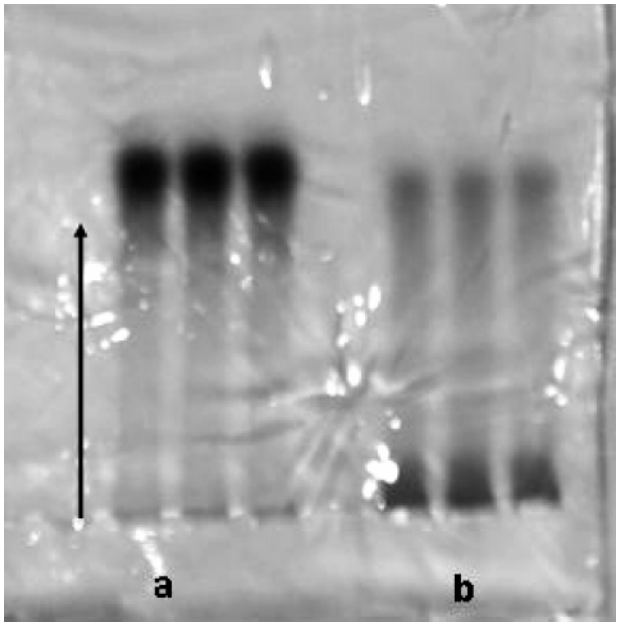

Figure 8. Electrophoresis of (a) citric acid coated magnetic particles, (b) dye-bound magnetic particles.

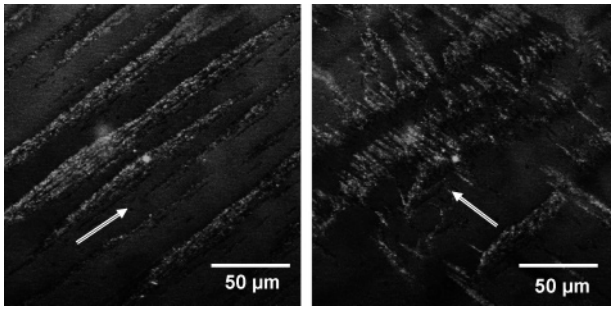

Figure 9. Confocal microscope fluorescence images of magnetic particles labeled with Rhodamine 110. The arrows in the pictures show the direction of the magnetic field.

Figure 7b. This curve provides a baseline for the measurements of the fluorescence anisotropy of the MP−CA-dye samples.

Adsorption of citric acid on the surface of the particles renders the surface negatively charged. This is demonstrated by the response of the particles to an electric field. Figure 8 shows results of electrophoresis measurements done on the MP−CA and also on the dye-bound MP−CA. The particles moved from their initial position toward the anode up to a distance of 40 mm in 1 h at an applied voltage of 80 V. In the dye-bound MP−CA, this movement was restricted and there was a clear gradient of concentration along the channel. This is expected because the dye-binding phenomenon results in partial annihilation of surface charges, thus reducing the mobility of the particles in an electric field. In an indirect way, thus, the electrophoresis result also confirms the binding of the dye onto the surface of the particles.

Figure 9 provides additional evidence of the binding of the dye to the particles and also demonstrates manipulation of the particles by an applied magnetic field. A suspension of fluorescently tagged particles was placed in a Petri dish filled with water, and a magnetic field (∼0.4 T) was applied. The confocal image shows parallel lines in the fluorescence image that are consistent with the alignment of the particles with the applied field. Upon switching the field orientation to the orthogonal direction, the alignment of the particles changes, and the fluorescence image also changes to parallel patterns in the orthogonal direction, which would be possible only if the fluorescent dye is bound to the particles. An unbound dye would produce a simple diffuse fluorescence that would not respond to the magnetic field.

To check whether fluorescently labeled MP−CA particles can be optically tracked in vitro, KB cells were incubated with MP−CA particles and then imaged as described above. Transmission and fluorescence images are shown in Figure 10. These images demonstrate that the fluorescent particles are efficiently taken up by the cells. Moreover, the fluorescence pattern seen in Figure 10b is quite similar to that of cells stained with free rhodamine 110 (Figure 10c). Rhodamine dyes are well-known stains for mitochondria. Thus, the rhodamine molecules bound to the surface of particles retain, to some extent, their ability to interact with the surface of mitochondria, as free dye molecules do.[30] Furthermore, this suggests that other functional molecules can be bound to the surface of magnetic particles without significant degradation of their functionality.

These experiments collectively indicate that the amount of free dye in the multiply washed sample of the fluorescently labeled nanoparticles is negligible. This is reinforced by the observation that the fluorescence images of the cells moved in response to a magnetic field, while the ones due to neat rhodamine 110 would not. A short movie of this motion is included in the Supporting Information for this manuscript, showing the cells of Figure 10b moving toward the lower left in response to the application of a magnetic field.

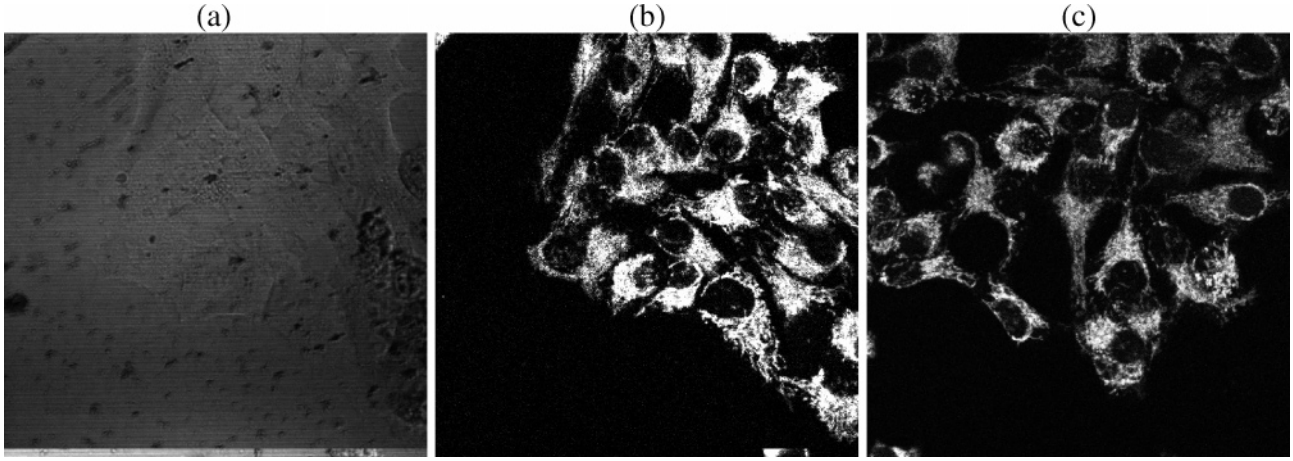

Figure 10. (a) Transmission image of KB cells with MP−CA ingested. (b) Fluorescence image of KB cells treated with fluorescently labeled MP−CA particles. (c) Fluorescence image of cells treated with Rhodamine 110 alone.

Summary and Conclusions

In summary, the results presented herein demonstrate that the surface of magnetite nanoparticles can be stabilized in an aqueous dispersion by the adsorption of citric acid. The citric acid may be adsorbed on the surface of the magnetite nanoparticles by coordinating via one or two of the carboxylate functionalities, depending on steric necessity and the curvature of the surface. This leaves at least one carboxylic acid group exposed to the solvent, and this group should be responsible for making the surface charged and hydrophilic. Further, the presence of a terminal carboxylic group provides an avenue to extended bond formation with fluorescent dyes, proteins, hormone linkers, and other molecules so that specific targeting within biological systems can be facilitated. We have shown that rhodamine 110 dye can be bound to the surface of these particles by standard procedures and still retain its fluorescence. Such fluorescently labeled magnetic particles can be taken up by cultured cells in vitro and optically tracked using confocal fluorescence microscopy. Finally, because of the small sizes of the nanoparticles, their stable dispersion in aqueous medium, the presence of carboxyl groups on their surfaces, and the magnetic characteristics of the particles, the biocompatible ferrofluid presented here should be of considerable value in numerous areas of biomedical research including bioingestion, magnetophoretic control, and bioimaging.

Acknowledgment. The authors thank Shumin Wang and Hong Luo for providing the magnetization data. Financial support from the UB office of the Vice President for Research, the National Science Foundation REU program, and a DURINT grant from the Chemistry and Life Sciences Division of the Air Force Office of Scientific Research are acknowledged.

Supporting Information Available: This material is available free of charge via the Internet at http://pubs.acs.org.

References and Notes

(1) (a) Bean, C. P.; Livingstone, J. D. *J. Appl. Phys*. **1959**, *30*, 120S. (b) Neel, L. *Rev. Mod. Phys*. **1953**, *25*, 293.

(2) (a) Held, G. A.; Grinstein, G.; Doyle, H.; Sun, S.; Murray, C. B. *Phys. Rev. B* **2001**, *64*, 012408. (b) Luo, W.; Nagel, S. R.; Rosenbaum, T. F.; Rosenweig, R. E. *Phys. Rev. Lett*. **1991**, *67*, 2721.

(3) (a) Molotkov, S. N.; Nazin, S. S. *Phys. Low-Dimens. Struct*. **1997**, *10*, 85. (b) Weisendanger, R. *MRS Bull*. **1997**, *22*, 31.

(4) (a) Poddar, P.; Fried, T.; Markovich, G. *Phys. Rev. B* **2002**, *65*, 172405. (b) Black, C. T.; Murray, C. B.; Sandstrom, R. L.; Sun, S. *Science* **2000**, *290*, 1131.

(5) (a) Fertman, V. E. *Magnetic Fluids Guide Book: Properties and Applications*; Hemisphere Publishing Co: New York, 1990. (b) Berkovsky, B. M.; Medvedev, V. F.; Krakov, M. S. *Magnetic Fluids: Engineering Applications*; Oxford University Press: Oxford, 1993. (c) Raj, K.; Moskowitz, B.; Casciari, R. *J. Magn. Magn. Mater*. **1995**, *149*, 174.

(6) (a) Ziolo, R. F.; Giannelis, E. P.; Weinstein, B. A.; O'Horo, M. P.; Ganguly, B. N.; Mehrotra, V.; Russell, M. W.; Huffman, D. R. *Science* **1992**, *257*, 219. (b) Hyeon, T. *Chem. Commun*. **2003**, *8*, 927. (c) Murray, C. B.; Sun, S.; Gaschler, W.; Dolyle, H.; Betley, T. A.; Kagan, C. R. *IBM J. Res. Dev*. **2001**, *45*, 47.

(7) (a) Choi, J.-W.; Ahn, C. H.; Bhansali, S.; Henderson, H. T. *Sens. Actuators* **2000**, *68*, 34. (b) Choi, J.-W. T.; Liakopoulos, M. *Biosens. Bioelectron*. **2000**, *16*, 409.

(8) (a)Pankhurst, Q. A.; Connolly, J.; Jones, S. K.; Dobson, J. J. Phys. D: Appl. Phys. 2003, 36, R167. (b) Safarýk, I.; Safarýkova, M. In *Scientific and Clinical Applications of Magnetic Carriers*; Hafeli, U., Schutt, W., Teller, J., Zborowski, M., Eds.; Plenum Press: New York, 1997.

(9) Plank, C.; Schillinger, U.; Scherer, F.; Bergemann, C.; Remy, J. S.; Krotz, F.; Anton, M.; Lausier, J.; Rosenecker, *J. Biol. Chem*. **2003**, *384*, 737.

(10) Roger, J.; Pons, J. N.; Massart, R.; Halbreich, A.; Bacri, J. C. *Euro. Phys. J. Appl. Phys*. **1999**, *5*, 321.

(11) Koenig, S. H.; Kellar, K. E. *Academic Radiology* **1996**, *3*, 273.

(12) Leslie-Pelecky, D. L.; Rieke, R. D. *Chem. Mater*. **1996**, *8*, 1770.

(13) Suzuki, M.; Shinkai, M.; Kamihira, M.; Kobayashi, T. *Biotech. Appl. Biochem*. **1995**, *21*, 335.

(14) (a) Karumanchi, R. S. M. S.; Doddamane, S. N.; Sampangi, C.; Todd, P. W. *Trends Biotechnol*. **2002**, *20*, 72. (b) Mirowski, E.; Moreland, J.; Russek, S. E.; Donahue, M. J. *Appl. Phys. Lett*. **2004**, *84*, 1786.

(15) (a) Prasad, P. N. *Introduction to Biophotonics;* John Wiley & Sons: New York, 2003. (b) Prasad, P. N. *Nanophotonics*; John Wiley & Sons: New York, 2004. (c) Levy, L.; Sahoo, Y.; Kim, K.; Bergey, E. J.; Prasad, P. N. *Chem. Mater*. **2002**, *14*, 3715.

(16) Vayssieres, L.; Chaneac, C.; Troc, E.; Jolivet, J. P. *J. Colloid Interface Sci*. **1998**, *205*, 205.

(17) Colvin, V. L.; Goldstein, A. N.; Alivisatos, A. P. *J. Am. Chem. Soc*. **1992**, *114*, 5221.

(18) Fried, T.; Shemer, G.; Markovich, G. *Adv. Mater*. **2001**, *13*, 1158.

(19) Sahoo, Y.; Pizem, H.; Fried, T.; Golodnitsky, D.; Burstein, L.; Sukenik, C. N.; Markovich, G. *Langmuir* **2001**, *17*, 7907.

(20) Shen, L. P.; Laibinis, E.; Hatton, T. A. *Langmuir* **1999**, *15*, 447.

(21) Joseph, S.; Olbrich, C.; Kirsch, J.; Hasbach, M.; Briel, A.; Schirner, M. *Pharm. Res*. **2004**, *21*, 920.

(22) Anderson, G. W.; Zimmerman, J. E.; Callahan, F. M. *J. Am. Chem. Soc*. **1964**, *86*, 1839.

(23) Wagner, C. D.; Riggs, R. M.; Davis, L. E.; Moulder, J. F. *Handbook of Electron Spectroscopy*; Muilenberg, G. E., Ed.; Perkin-Elmer Corp., Physical Electronics: Eden Prairie, MN, 1979.

(24) (a) Okudera, H.; Toraya, H. Z. *Kristallografiya* **1998**, *231*, 461. (b) Sadykov, V. A.; Isupova, L. A.; Tsybulya, S. V.; Cherepanova, S. V.; Litvak, G. S.; Burgina, E. B.; Kustova, G. N.; Kolomiichuk, V. N.; Ivanov, V. P.; Paukshtis, E. A.; Golovin, A. V.; Avvakumov, E. G. *J. Solid State Chem*. **1996**, *123*, 191.

(25) Todorovsky, D. S.; Dumanova, D. G.; Todorovska, R. V.; Getsova, M. M. *Croat. Chem. Acta* **2002**, *75*, 155.

(26) (a) Kallay, N.; Matijevic, E. *Langmuir* **1985**, *1*, 195. (b) Zhang, Y.; Kallay, N.; Matijevic, E. *Langmuir* **1985**, *1*, 201.

(27) Badia, A.; Cuccia, L.; Demers, L.; Morin, F.; Lennox, R. B. *J. Am. Chem. Soc*. **1997**, *119*, 2682.

(28) Lakowicz, J. R. *Principles of fluorescence spectroscopy*; Plenum Press: New York, 1983.

(29) White, C. E.; Argauer, R. J. *Fluorescence Analysis-A Practical Approach*; Marcel Dekker: New York, 1970.

(30) Haughland, R. P. *Molecular Probes: Handbook of Fluorescent Probes and Research Chemicals*; Molecular Probes Inc.: Eugene, OR, 2002.